



Deposited via The University of York.

White Rose Research Online URL for this paper:

<https://eprints.whiterose.ac.uk/id/eprint/152477/>

Version: Published Version

---

**Article:**

Xiao, Y., Go, S., Grzywacz, R. et al. (2019) Search for  $\alpha$  decay of Te 104 with a novel recoil-decay scintillation detector. Physical Review C. 034315. ISSN: 2469-9993

<https://doi.org/10.1103/PhysRevC.100.034315>

---

**Reuse**

Items deposited in White Rose Research Online are protected by copyright, with all rights reserved unless indicated otherwise. They may be downloaded and/or printed for private study, or other acts as permitted by national copyright laws. The publisher or other rights holders may allow further reproduction and re-use of the full text version. This is indicated by the licence information on the White Rose Research Online record for the item.

**Takedown**

If you consider content in White Rose Research Online to be in breach of UK law, please notify us by emailing [eprints@whiterose.ac.uk](mailto:eprints@whiterose.ac.uk) including the URL of the record and the reason for the withdrawal request.

## Search for $\alpha$ decay of $^{104}\text{Te}$ with a novel recoil-decay scintillation detector

Y. Xiao,<sup>1</sup> S. Go,<sup>1,2</sup> R. Grzywacz,<sup>1,3</sup> R. Orlandi,<sup>4</sup> A. N. Andreyev,<sup>4,5</sup> M. Asai,<sup>4</sup> M. A. Bentley,<sup>5</sup> G. de Angelis,<sup>6</sup> C. J. Gross,<sup>3</sup> P. Hausladen,<sup>3</sup> K. Hirose,<sup>4</sup> S. Hofmann,<sup>7</sup> H. Ikezoe,<sup>4</sup> D. G. Jenkins,<sup>5</sup> B. Kindler,<sup>7</sup> R. L guillon,<sup>4</sup> B. Lommel,<sup>7</sup> H. Makii,<sup>4</sup> C. Mazzocchi,<sup>8</sup> K. Nishio,<sup>4</sup> P. Parkhurst,<sup>9</sup> S. V. Paulauskas,<sup>1</sup> C. M. Petrache,<sup>10</sup> K. P. Rykaczewski,<sup>3</sup> T. K. Sato,<sup>4</sup> J. Smallcombe,<sup>4</sup> A. Toyoshima,<sup>4</sup> K. Tsukada,<sup>4</sup> K. Vaigneur,<sup>11</sup> and R. Wadsworth<sup>5</sup>

<sup>1</sup>*Department of Physics and Astronomy, University of Tennessee, Knoxville, Tennessee 37996, USA*

<sup>2</sup>*Department of Physics, Kyushu University, Fukuoka 819-0395, Japan*

<sup>3</sup>*Physics Division, Oak Ridge National Laboratory, Oak Ridge, Tennessee 37831, USA*

<sup>4</sup>*Advanced Science Research Center, Japan Atomic Energy Agency, Tokai, Ibaraki 319-1195, Japan*

<sup>5</sup>*Department of Physics, University of York, Heslington, York YO10 5DD, United Kingdom*

<sup>6</sup>*Istituto Nazionale di Fisica Nucleare - Laboratori Nazionali di Legnaro, Legnaro PD 35020, Italy*

<sup>7</sup>*GSI Helmholtz Centre for Heavy Ion Research, Darmstadt 64291, Germany*

<sup>8</sup>*Faculty of Physics, University of Warsaw, Warszawa PL 02-093, Poland*

<sup>9</sup>*Proteus, Inc., Chagrin Falls, Ohio 44022, USA*

<sup>10</sup>*Centre de Sciences Nucl aires et Sciences de la Mati re, CNRS/IN2P3, Universit  Paris-Saclay, 91405 Orsay, France*

<sup>11</sup>*Agile Technologies, Knoxville, Tennessee 37932, USA*



(Received 5 August 2018; revised manuscript received 31 July 2019; published 16 September 2019)

A search for superallowed  $\alpha$  decay of  $N = Z$  nuclei  $^{104}\text{Te}$  and  $^{108}\text{Xe}$  was carried out using a novel recoil-decay scintillator detector at the tandem accelerator facility at the Japan Atomic Energy Agency (JAEA). Inorganic crystal scintillation material YAP:Ce (yttrium aluminum perovskite) coupled to a position-sensitive photomultiplier tube (PSPMT) was implemented for the first time in a radioactive decay experiment. Residues from the fusion-evaporation reaction  $^{58}\text{Ni} + ^{54}\text{Fe} \rightarrow ^{112}\text{Xe}^*$  were separated by the JAEA Recoil Mass Separator (RMS) and implanted into the YAP:Ce crystal.  $\alpha$  decays of neutron-deficient tellurium isotopes were identified and proton emission of  $^{109}\text{I}$  was observed. The  $\alpha$ -decay chain  $^{109}\text{Xe} \rightarrow ^{105}\text{Te} \rightarrow ^{101}\text{Sn}$  was recorded with a time interval of 960 ns between two  $\alpha$  pulses. Position localization in the crystal for decays and ions in the energy range from hundreds of keV to 60 MeV was achieved with an accuracy of 0.67 mm, proving that this detector is capable of making temporal and spatial correlations for fast decay events. No conclusive evidence was found for the decay chain  $^{108}\text{Xe} \rightarrow ^{104}\text{Te} \rightarrow ^{100}\text{Sn}$  within 3 days of experiment. However, two events were observed with properties consistent with the reported observation at the Fragment Mass Analyzer (FMA), but with a separation between signals of less than 4 ns. The cross section limit of 130 pb was obtained for production of two events of  $^{108}\text{Xe}$ , about an order of magnitude below the expectation based on earlier cross section measurements and the HIVAP fusion-evaporation code.

DOI: [10.1103/PhysRevC.100.034315](https://doi.org/10.1103/PhysRevC.100.034315)

### I. INTRODUCTION

In the  $\alpha$ -decay island northeast of  $^{100}\text{Sn}$ , valence protons and neutrons are expected to occupy the same single-particle orbitals outside the  $N = Z = 50$  doubly magic nucleus  $^{100}\text{Sn}$ . The additional interaction between protons and neutrons may lead to the enhanced pre-formation of an  $\alpha$  particle and therefore to the enhancement of  $\alpha$ -decay probability, the so-called superallowed  $\alpha$  decay [1]. Extensive experimental efforts have been made in this region, providing evidence of such enhancement [2–6]. The ultimate evidence would be the observation of accelerated  $\alpha$  decay of  $^{104}\text{Te}$  ( $N = Z = 52$ ) with two protons and two neutrons occupying the same single-particle orbitals. When  $\alpha$  clusterization is included, the estimated half-life would be as short as 50 ns [7], which makes the measurement of  $^{104}\text{Te}$  decay very difficult. The indirect production of this isotope through the synthesis of the longer-lived  $\alpha$ -decay precursor  $^{108}\text{Xe}$ , whose half-life is

estimated to be 0.15 ms [7] by the same model with enhanced preformation, would enable the study of  $^{104}\text{Te}$  using the in-flight electromagnetic separation technique. Even in this case, the short half-life of  $^{104}\text{Te}$  is a challenge for today's detection techniques and requires the use of a fast response detection method to be able to separate the  $\alpha$  decay of  $^{108}\text{Xe}$  and the fast  $\alpha$  decay of  $^{104}\text{Te}$ . Semiconductor detectors, e.g., double-sided strip detectors (DSSDs), are widely used as implantation detectors for such measurements of ions and charged particle emission. One of the shortcomings of semiconductor detector technology is its relatively slow response. The use of digital signal processing techniques [8,9], overcame some of the limitations related to the slow response of silicon, but crossing the 100 ns limit to resolve two consecutive pulses remains a challenge. In addition, the expensive DSSDs are susceptible to radiation damage. A recent measurement [10] resulted with the half-life estimate  $T_{1/2} < 18$  ns for  $^{104}\text{Te}$  based on

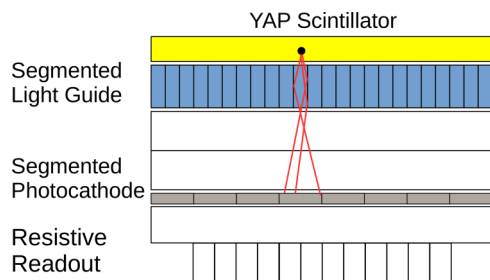


FIG. 1. Schematic illustration of YAP:Ce segmented detector. See text for details.

two  $^{108}\text{Xe}$  decays. The result of this experiment exemplified the challenges of performing the experiment searching for  $^{104}\text{Te}$  using DSSDs. A very large enhancement of the  $\alpha$ -decay probability was suggested [10]. This result needs to be independently confirmed and measured with improved statistics and accuracy.

In this work, we propose a new, alternative approach to overcome the limitations of semiconductor detectors and use a fast response scintillator for detection of short-lived radioactivities. Scintillators provide the ability to record successive recoil and decay signals with much shorter time intervals than can be achieved by semiconductor detectors, at the cost of worse energy resolution. Another advantage of scintillator of this type described here is its resistance to radiation damage.

The production cross section of  $^{108}\text{Xe}$  in the fusion-evaporation  $^{58}\text{Ni} + ^{54}\text{Fe}$  reaction is predicted by HIVAP code to be of the order of 1 nb [11,12], while the isobaric background can be as high as hundreds of mb. High intensity primary beams, which may result in high rate of implantation of unwanted ions, are needed to compensate for the low production cross section. The use of fast radiation-hard segmented scintillators provides a solution also for this experimental challenge. An example of such a detector utilizing a plastic scintillator was developed [13] and implemented as a fast trigger in  $\beta$ -decay experiments [14]. The detector concept presented here can also be used in superheavy element search experiments, in cases where very short lifetimes are expected. The detector is described in Sec. II while its use for studying neutron-deficient  $\alpha$  and proton emitters in the  $^{100}\text{Sn}$  region is illustrated in Sec. III. Section IV gives a summary and outlook on future studies.

## II. DETECTOR SYSTEM

The concept of using the thin inorganic scintillator YAP:Ce (yttrium aluminum perovskite) was proposed as a dedicated  $\alpha$ -particle detector for a  $d$ - $t$  generator [15,16]. We use a similar design but with new experimental functionalities required for ion-decay correlations, traditionally implemented using DSSD-based experiments. The detector consists of three parts: a YAP:Ce crystal, a quartz segmented light guide with diffuser, and a Hamamatsu position-sensitive photomultiplier tube (PSPMT), as shown in Fig. 1. The 50.8 mm (2 inch) diameter 1 mm thick piece of YAP:Ce crystal was coupled to the quartz light guide with optical cement and polished

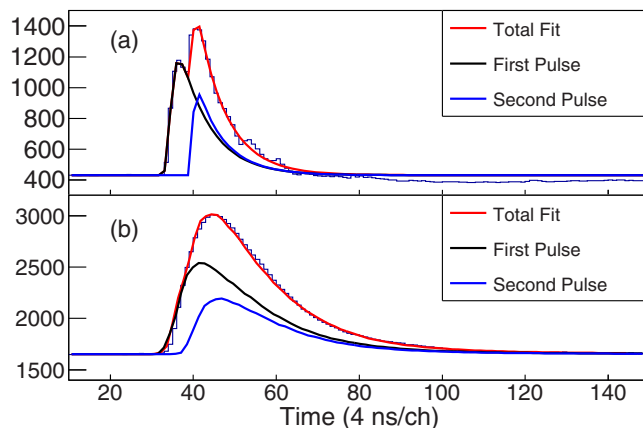


FIG. 2. Typical recorded traces of successive decays with rise time of 10 ns and time interval of 17 ns dynode signal and corresponding anode signals are shown in (a) and (b) respectively. Anode pileup pulses with slow rise time can be decomposed using the timing information from the dynode and fitted averaged anode pulses.

down to 500  $\mu\text{m}$ . The light guide was segmented into 24 by 24 pixels, with the size of each pixel being  $2 \times 2 \text{ mm}^2$ . The PSPMT reads the light from the YAP crystal with a dynode readout providing fast timing signals and four anode readouts for evaluation of energies and positions of signals. The YAP:Ce crystal was chosen as the material for building such a detector due to its good performance at fast timing [17]. The very short scintillation decay time for this crystal [18] makes it possible to observe successive events within less than 100 ns time difference. Figure 2 shows an example of a captured trace with a time difference of 17 ns between two pulses. The smallest time interval of the pileup traces recorded and resolved in our experiment was 13 ns. The main limitation to resolve two signals comes from the low-pass Nyquist filter of the Pixie-16 digitizer operating at 250 megasamples per second (MSPS), which has about 125 Hz cutoff frequency. As shown in Fig. 2, every signal has about 10 ns rise time, which is due to this effect. By fitting raw traces from the dynode readout with the averaged decay pulse shape, it is, however, still possible to resolve pileup pulses with time interval shorter than 20 ns. To obtain the position information, this fit procedure has to be performed separately for all four anode traces. For two pulses in the same pixel, the ratio of the amplitude of the first pulse to that of the second one should be the same for all anode traces as the ratio in dynode trace. Otherwise, this ratio will be different, implying different positions of two pulses. In this experiment, we did not find pileup pulses in the same pixel with time interval shorter than 20 ns.

The response of the detector to  $\alpha$ -particle interaction and light propagation was described, e.g., by Zhang *et al.* [16]. In brief, when a charged particle is implanted into the YAP:Ce crystal, scintillation photons are generated through atomic interactions. These photons are guided through the pixel of the optical guide and scattered, and are registered by multiple photocathodes of the flat panel photomultiplier. The 64 segments of the Hamamatsu H8500 PSPMT were read using Anger logic to reduce the number of channels

required to reconstruct the position of the interaction. The fast sampling analog-to-digital converter implemented in the Pixie-16 data acquisition module [19] digitized the PSPMT signals. The pulse shape was recorded for each implantation or decay event. During the majority of the measurement time, the surface of the YAP:Ce crystal was covered by a  $1.6\ \mu\text{m}$  thick aluminum foil to increase the efficiency of collection of scintillation photons and also to degrade the energy of the implanted ions. Therefore, induced signals of ions are pushed below those of the expected  $\alpha$  particles to reduce the background for radioactive decay. The energy loss of charged particles and ions passing through this layer was corrected during the calibration. The center-of-gravity algorithm was applied to reproduce the position of an event inside the YAP:Ce crystal based on the integration over light-induced electric pulse. By comparing the charge collected from the upper two anodes to the total charge collected, the normalized vertical position of this signal can be determined. A similar method is applied to deduce the normalized horizontal position of a signal by reading the changes collected from the right two anodes:

$$x = \frac{\sum_{\text{right}} Q}{\sum_{\text{all}} Q}, \quad y = \frac{\sum_{\text{upper}} Q}{\sum_{\text{all}} Q} \quad (1)$$

An  $^{241}\text{Am}$   $\alpha$  source was used to test the capability of the position sensitivity of the detector system. In Figure 3(a), the raw position of the hit pattern of  $\alpha$  particles is shown in part (i). Slight barrel distortion is present, which can be corrected for in the post-processing. Position correction was implemented using a third-order polynomial, which gives a pattern with even distances between adjacent segments reflecting segmentation on the optical guide. The projection of the two-dimensional (2D) map onto the  $x$  axis is shown in part (ii) of Fig. 3(a). The average FWHM of these peaks is  $0.67\ \text{mm}$ , much less than the actual dimension of a pixel on the optical guide of  $2\ \text{mm}$  which is due to the optical transformation of the system. This means that the detector system achieved the necessary spatial resolution required to assign the location of the interaction to the specific light-guide segment. The distribution of signals per pixel after correction is shown in Fig. 3(b).

The number of scintillation photons reflects the amplitude of the signal induced by the implanted charged particles or decays. Therefore, the energy is determined from the integration of the four position pulses. Due to imperfections of the scintillator, light guide and PSPMT photocathode inhomogeneities, and use of the Anger logic, it is necessary to apply energy gain-match for each pixel. Figures 4(a) and 4(b) show a comparison between position of pixels versus energy spectra before and after gain-match, where two-dimensional distribution of pixels has now been converted into one dimension using the following algorithm:  $N_{\text{pixel}} = M_{\text{row}} \times 24 + M_{\text{column}}$ . Figure 4(c) shows the projection of all signals onto the  $x$  axis. There are 443 pixel calibrated while the remaining 133 edge pixels were omitted due to lack of statistics to fit a peak due to the circular shape of the active scintillator surface. The energy resolution at  $5485.6\ \text{keV}$  of the  $^{241}\text{Am}$   $\alpha$  decay line is about  $430\ \text{keV}$ , i.e.,  $7.8\%$  FWHM. This is a typical value for a YAP:Ce scintillator [18].

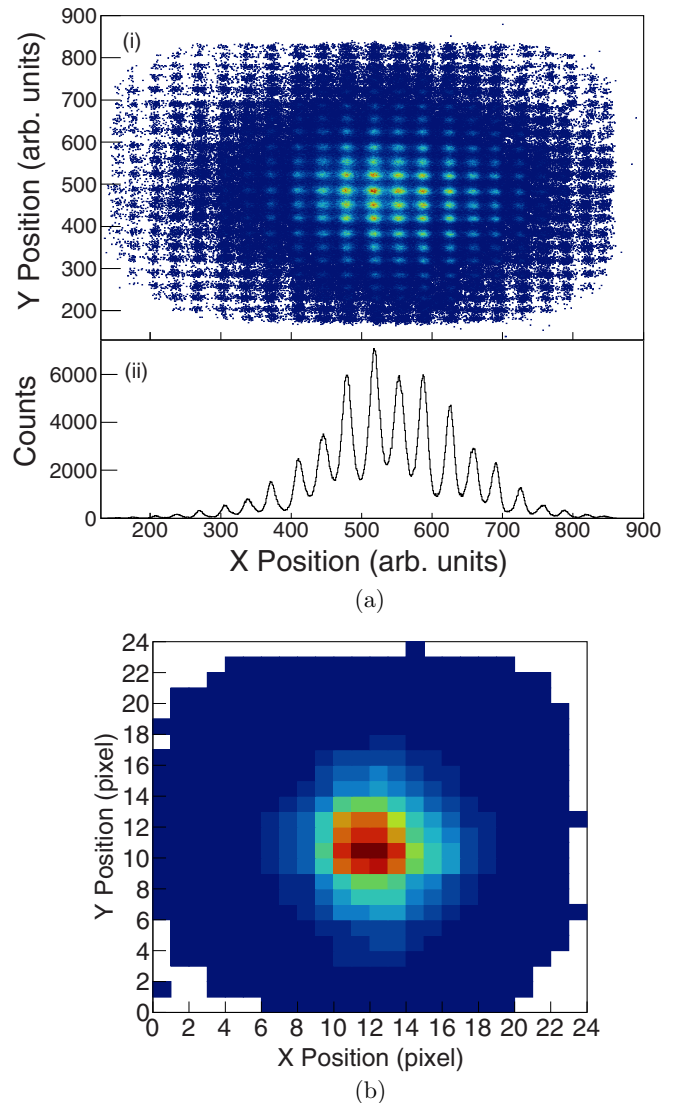


FIG. 3. (a) Raw position distribution of signals reproduced by the center-of-gravity method plotted in arbitrary dimension units is displayed in part (i). The projection of the two-dimensional histogram from part (i) onto the  $x$  axis is shown in part (ii). The shape of each peak is well defined and they are well separated. (b) The pixelated 2D distribution of signals.

### III. STUDIES OF NEUTRON-DEFICIENT ISOTOPES IN THE FUSION-EVAPORATION REACTION

The critical development presented here is the ability for the segmented YAP:Ce detector to detect recoil-decay correlations. This capability was demonstrated for the short-lived  $\alpha$  and proton emitters in the  $^{100}\text{Sn}$  region. The experiment searching for the  $^{108}\text{Xe} \rightarrow ^{104}\text{Te} \rightarrow ^{100}\text{Sn}$  decay chain and a brief measurement of  $^{109}\text{Xe}$  decay took place at the tandem accelerator facility of the Japan Atomic Energy Agency (JAEA) in Tokai Japan. A primary beam of  $^{58}\text{Ni}$  at an energy of  $250\ \text{MeV}$  was used. A segmented enriched  $^{54}\text{Fe}$  target with  $550\ \mu\text{g}/\text{cm}^2$  thickness (self-supporting) was made by a rolling method in the GSI (Darmstadt) target laboratory. It was rotated to enable acceptance of the beam

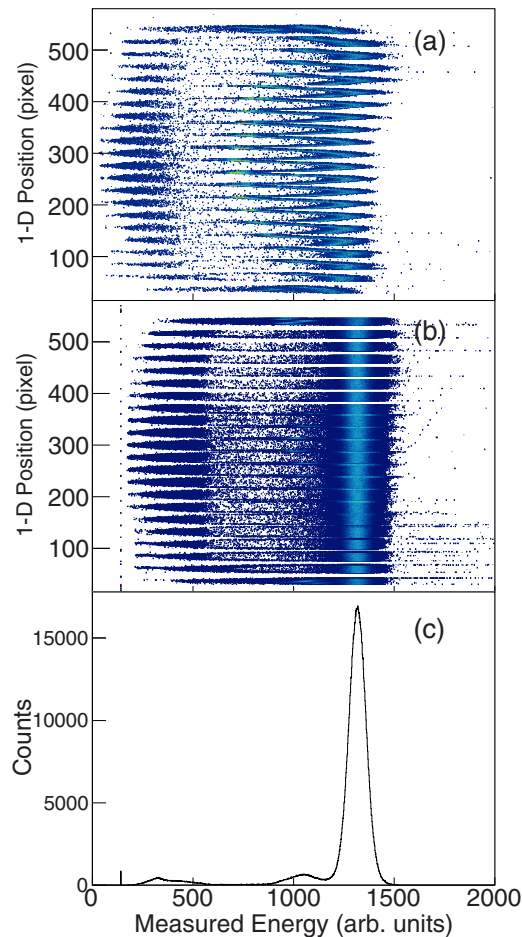


FIG. 4. (a) The  $N_{\text{pixel}}$  position vs integral of the trace induced by charged particles in the PSPMT (QDC) spectrum before the energy gain-match. (b) The  $N_{\text{pixel}}$  position vs QDC after gain-match. (c) A projection of the distribution of measured energy of  $^{241}\text{Am}$   $\alpha$  particles. See text for details.

with an average intensity of 12 p nA. Four target segments were mounted on a rim of the rotating frame, which gives the target-center diameter 134 mm. The beam was deflected while the target frame ran over the beamline to avoid the scattering background generated by interaction of the beam with the segmented target frame. The reaction residues were separated by the Recoil Mass Separator (RMS) [20] and were implanted into the YAP:Ce detector at the focal plane of the RMS. Upstream from the YAP:Ce detector, a multiwire proportional chamber (MWPC) was installed followed by a narrow vertical slit. The MWPC provided a signal associated with ion implantation in YAP:Ce and was used to tag events as recoils, while decays did not have any associated signal from the MWPC. The PSPMT was glued with a vacuum grade epoxy into an aluminum flange and served as the sole barrier between air and vacuum of the RMS. The vacuum chamber containing YAP:Ce was surrounded by a large NaI detection array, which covered half of the solid angle around the implantation detector. The most abundant contaminants in this experiment were  $\beta^+$  emitters, which finally led to a pair of 511 keV photons from positron annihilation. The NaI

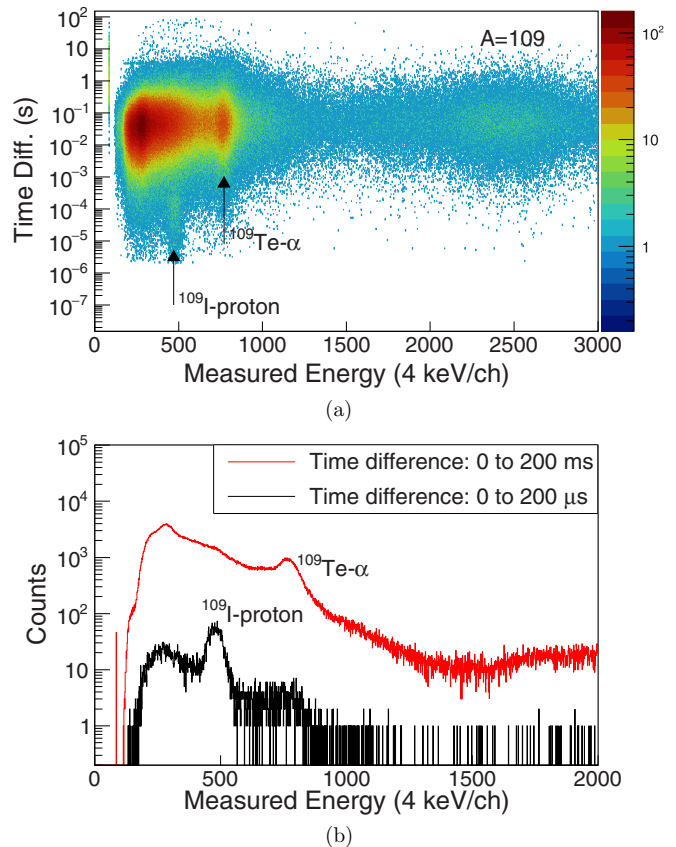


FIG. 5. (a) In the 2D histogram, the y axis is the time difference between the preceding ion and the subsequent decay shown in logarithmic scale, while the x axis shows the measured energy of the  $\alpha$  decay event. (b) This 1D histogram is the projection of the 2D histogram above, gating on different time range. It shows proton emission of  $^{109}\text{I}$  and  $\alpha$  decay of  $^{109}\text{Te}$ .

detection array in this configuration was used to veto  $\beta$  decays and related particle and  $\gamma$ -ray emissions.

For the YAP:Ce detector, during most of the time, recording of pulse shapes (traces) was enabled only for signals in anticoincidence with the MWPC, identified as decays only, to reduce the data volume. Trapezoidal filters were implemented in the field programmable array gate (FPGA) for local triggering of signals and assignment of time stamps [19].

By changing the settings of the RMS and the width of the selection slits at the exit of the RMS, the implanted ions were selected by mass-to-charge ratio among the neutron-deficient tellurium isotopes  $^{107,108,109}\text{Te}$ , which are the most abundant  $\alpha$  emitters produced. Therefore, the  $\alpha$  decays of these tellurium isotopes can be used to benchmark the detector and also as internal energy calibration. The energy distribution of  $\alpha$  decays of tellurium isotopes are shown in Figs. 5 and 6. Due to the high effective  $Z = 37$  and the thickness of 500  $\mu\text{m}$  of the YAP:Ce crystal,  $\beta$ -delayed protons and electrons contributed to the background on the left side of the  $\alpha$  peaks in both spectra. The energy resolutions for  $\alpha$  lines of  $^{108,109}\text{Te}$  are measured to be 8.2% and 8.0%. Because of the high average ion implantation rate, 3 kHz, the search for correlation for long-lived activities such as  $^{108}\text{Te}$  ( $T_{1/2} = 2.1$  s) and  $^{109}\text{Te}$

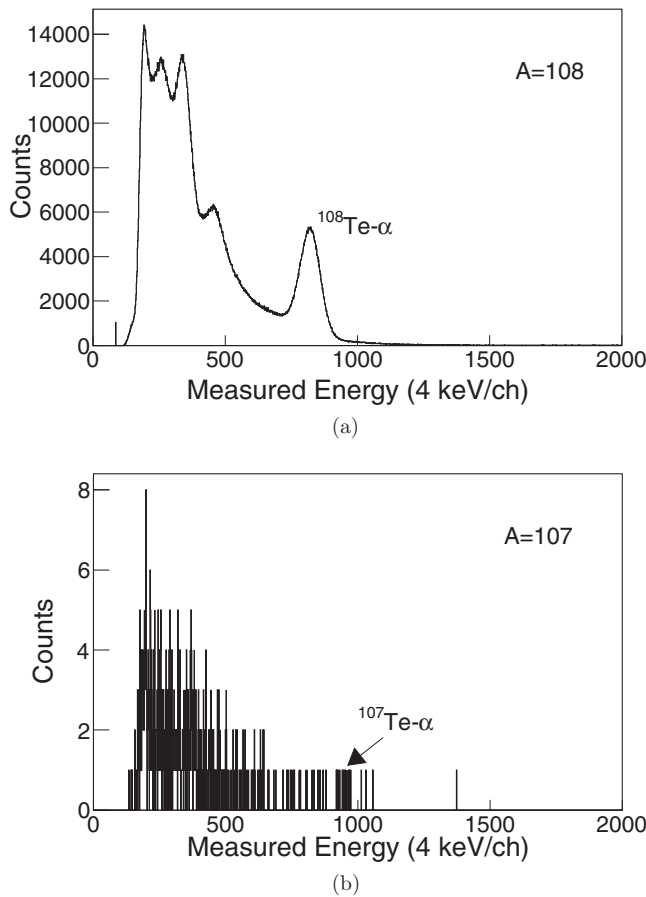


FIG. 6. The same as in Fig. 5(b), with the RMS settings optimized for mass number  $A = 108$  and a gate on time difference from 0 to 20 s (a) and  $A = 107$  with a time gate from 0 to 30 ms (b).

( $T_{1/2} = 4.6$  s) would not result in correct lifetime measurements, as would be the case also for a DSSD detector under the same experimental conditions. However, the fast response and radiation hardness of the YAP:Ce detector makes it an ideal tool for studying short-lived radioactivities ( $T_{1/2} < 1 \mu\text{s}$ ), for which it performs best. Within the time range up to 200  $\mu\text{s}$ , using settings for mass numbers 109 and 108, a fast decay component in the decay time vs energy spectrum emerges, as shown in Figs. 7 and 5. The half-life of the fast decay group is determined to be  $89.3 \pm 6.0 \mu\text{s}$  (see Fig. 8). This overlaps with the error bars of known half-life  $T_{1/2} = 93.5(3) \mu\text{s}$  for  $^{109}\text{I}$ ,  $b_p = 99.99\%$  [21]. Therefore, this group of decays is identified as ground-state proton emission of  $^{109}\text{I}$ , for which the proton energy is 810 keV [22]. The apparent amplitude of this signal is higher than would be expected from the  $\alpha$ -decay calibrations. This behavior is due to the fact that light yield for protons in YAP is higher than for  $\alpha$  particles and heavy ions [23]. The  $^{109}\text{I}$  proton line provides independent measurement of the YAP:Ce light yield response for protons.

Due to the fast scintillation decay constant of YAP:Ce, the detector is capable of recording two successive signals with short, submicrosecond time difference. This capability was exploited here with the use of a digital acquisition system. The measurement with the RMS ion-optics setting optimized

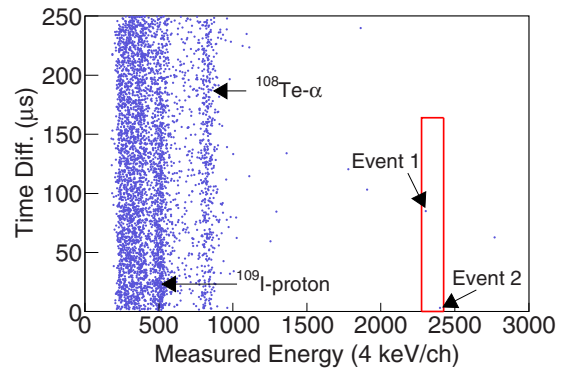


FIG. 7. The same 2D spectrum as displayed in Fig. 5(a), with the RMS settings optimized for mass number  $A = 108$ . The part enclosed by the red rectangle is the zone of interest for potential summed decay signals of  $^{108}\text{Xe}$  and  $^{104}\text{Te}$ . See text for details.

for transmission of  $A = 109$  ions lasted 4 hours. The aim was to search for  $\alpha$ -decay chain  $^{109}\text{Xe} \rightarrow ^{105}\text{Te} \rightarrow ^{101}\text{Sn}$  in order to verify the capabilities of this new detector. During that period, one event was recorded, which is in agreement with the cross section estimate [12]. The trace of successive signals from individual anode readouts is shown in Fig. 9. The energies of the first and second decays were determined to be 4290 and 4872 keV respectively. This is very close to the decay energies of the decay chain  $^{109}\text{Xe} \rightarrow ^{105}\text{Te} \rightarrow ^{101}\text{Sn}$ , where the strongest branches are 4063/3910 keV or 4880/4711 keV, depending on the decay path [5]. Note that since the energy resolution is around 8% for  $\alpha$  particles, their energy can be determined with an uncertainty of 160 keV. By gating on this trace and searching backward in time, the nearest ion implantation was found 2.87 ms prior to this signal and it appeared in the same pixel. This value is in agreement with the half-life for  $^{109}\text{Xe}$  of 13(2) ms. Thus, this complete decay chain is assigned to the decay of  $^{109}\text{Xe}$ .

For most of the beam time, the RMS setting was optimized for transmission of  $A = 108$  ions. The search for  $^{108}\text{Xe}$ , similarly to  $^{109}\text{Xe}$ , started with recording traces of two closely spaced successive decays. If such a trace was found, we would go backward in time to look for a preceding local ion. Only

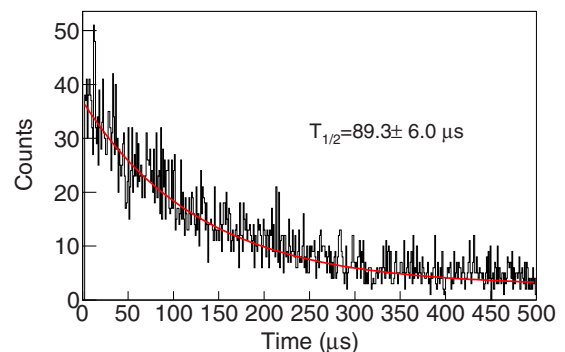


FIG. 8. Time distribution of the fast-decaying group from Fig. 5 identified as  $^{109}\text{I}$  proton decay. The red curve shows the exponential decay fit with linear background subtracted.

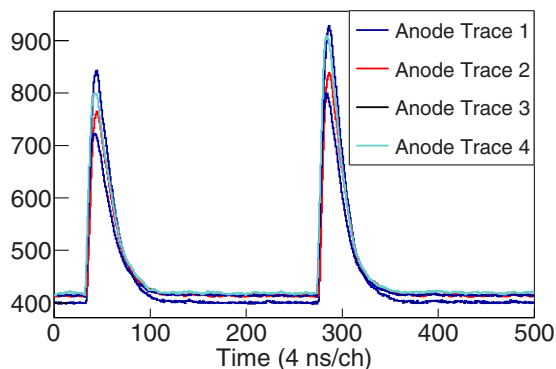


FIG. 9. The four traces of closely spaced pulses are independently collected from the four anode readouts, corresponding to the same successive  $\alpha$ -particle decay chain from  $^{109}\text{Xe}$ . By comparing the integral over QDC values of each pulse among the four traces, both the first and second decays were determined to be located in the same pixel.

3.4 days were available for this measurement. No conclusive trace for the decay chain  $^{108}\text{Xe} \rightarrow ^{104}\text{Te} \rightarrow ^{100}\text{Sn}$  was observed and no events indicating the lifetime of  $^{104}\text{Te}$  longer than 20 ns were observed. However, it is possible that two decay signals of  $^{108}\text{Xe}$  and  $^{104}\text{Te}$  are so close in time that they appear to be a large summed decay signal. Based on the ANL result [10], a region of interest for such summed signal correlated to ion implantations is shown in Fig. 7. Two events were observed inside but no pileup structure was observed in the second derivative of either trace. A similar analysis of the trace (see Fig. 10) would lead to  $T_{1/2} < 4$  ns for  $^{104}\text{Te}$ . The half-life of  $^{108}\text{Xe}$  from Fig. 10 would be  $30_{-12}^{+57}$   $\mu\text{s}$  calculated with the method described in [24]. The NaI veto and imposed time correlation gate dramatically reduces the background from  $\beta$  decays; see Fig. 11. Due to the presence of increased statistics of events in the region of interest around 9 MeV, we cannot exclude that the two observed events are due to signals induced by  $\beta$ -delayed proton emission, which were not completely eliminated by the anticoincidence gate

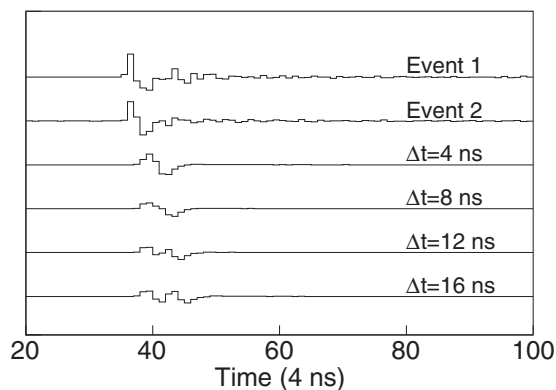


FIG. 10. The second derivative of traces of events 1 and 2 are compared to the second derivative of simulated traces of successive  $\alpha$  decays of  $^{108}\text{Xe}$  and  $^{104}\text{Te}$  with different time intervals.

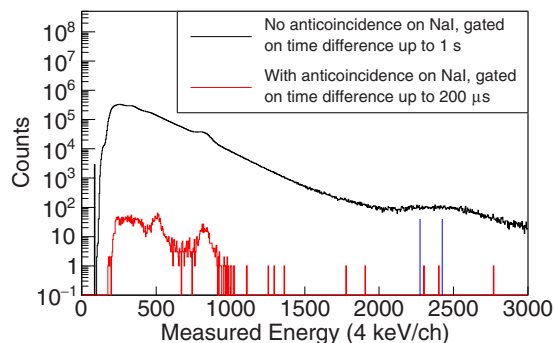


FIG. 11. Effect of the NaI anticoincidence gate imposed on the YAP correlated spectra. The black histogram shows the the total YAP energy distribution for the decays correlated to ion-implantation within 1 s. The red histogram shows the spectrum in anticoincidence with the NaI detector with the 200  $\mu\text{s}$  time gate on the ion-decay correlation. The borders of the energy range of interest are indicated by two vertical blue lines.

with the NaI veto detector. Therefore we cannot conclusively assign these events to  $^{108}\text{Xe}$  decay.

An upper limit of 130 pb was given for the cross section of  $^{108}\text{Xe}$  with a primary beam of  $^{58}\text{Ni}$  at 250 MeV bombarded on a 550  $\mu\text{g}/\text{cm}^2$  thick  $^{54}\text{Fe}$  target. The choice of the beam energy was based on the experimental systematics of the cross sections for Xe isotopes as discussed in [12]. Based on the  $^{109}\text{Xe}$  results, we expected an order-of-magnitude reduction of the production cross section for  $^{108}\text{Xe}$ . Our cross section limit of 130 pb for  $^{108}\text{Xe}$  is one order of magnitude smaller than the maximum cross section of 1 nb predicted by HIVAP [12], as was inferred for  $^{108}\text{Xe}$  in Ref. [12] based on  $^{109}\text{Xe}$  results [5,6]. This is similar (within a factor of 2) to the smaller cross section deduced from the ANL result [10].

Like all scintillators, the YAP:Ce crystal will have a variable light yield which will depend on different types of implanted charged particles [18]. Precise knowledge of the light yield, for the heavy ions, is critical to determine future detector design. This is particularly important in the recoil-decay experiment, where the heavy ions carry a lot more energy but can produce relatively less light than the lighter particles or  $\gamma$  rays.

Our experimental data set enables comparison of the light yields for  $\alpha$  particles, protons, and heavy ions. This can be achieved by comparing the position of discrete peaks of  $\alpha$  particles and protons from radioactive decays. We were able to extract the light yield and type or energy of implanted charged particles. As mentioned above,  $^{241}\text{Am}$   $\alpha$  particles implanted into the YAP:Ce crystal will experience loss in energy when passing through the aluminum foil attached to the surface of YAP:Ce crystal. The energy loss is evaluated to be 213 keV by comparing the position of  $\alpha$  line calibrated with  $\alpha$  lines of  $^{108,109}\text{Te}$  with the already known 5485.6 keV  $\alpha$ -decay energy of  $^{241}\text{Am}$ .

To determine the response of YAP:Ce for heavy ions, the aluminum foil was removed from the YAP:Ce crystal. A correlation matrix for correlated decays and preceding ions was set up [see Fig. 12(a)]. By gating on the proton group of  $^{109}\text{I}$ , a correlation between  $^{109}\text{I}$  recoils and protons can

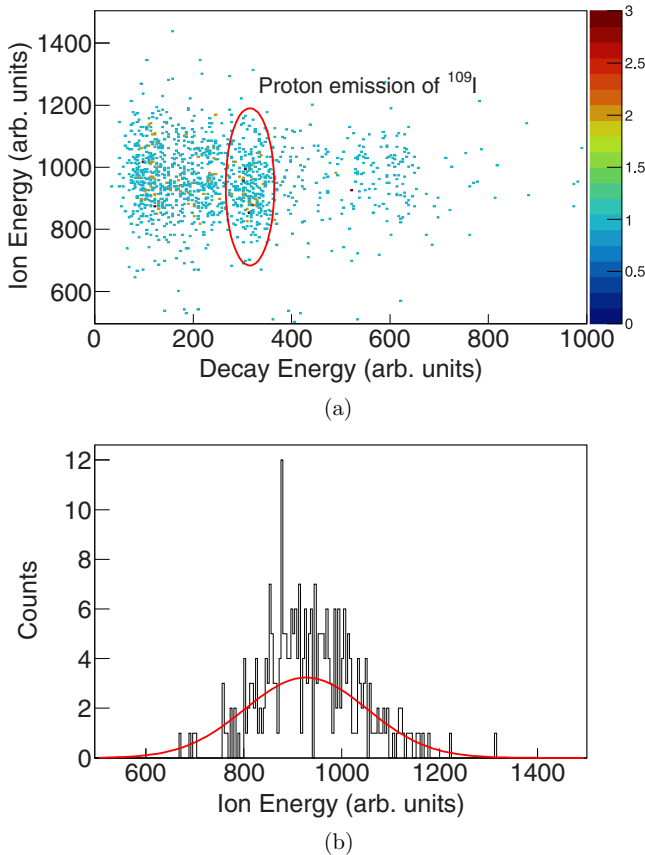


FIG. 12. (a) The correlation matrix for decays and preceding ions. Left to the  $^{109}\text{I}$  protons are the background produced by electrons and  $\beta$ -delayed protons. (b) The energy distribution of  $^{109}\text{I}$  ions in correlation with proton emissions is shown. The FWHM/centroid ratio is 27%, which is close to the energy dispersion of recoils from the RMS.

be identified. The energy of the  $^{109}\text{I}$  recoils deposited into YAP:Ce crystal can be calculated by subtracting the energy lost when passing through the MWPC. Therefore, the energy of  $^{109}\text{I}$  was determined to be 48 MeV with the energy resolution of 26% given by the RMS.

By comparing the  $\alpha$ -decay lines of  $^{108,109}\text{Te}$  and protons of  $^{109}\text{I}$ , the efficiency of light collection increases by a factor of 1.3 with the aluminum foil attached. The plot for light yield response shown in Fig. 13 is created from the data corresponding to the case with the aluminum foil attached. From Fig. 13, the conclusion is that the light yields of the YAP:Ce crystal for heavier charged particles decrease significantly. For the same species of particles, e.g.,  $\alpha$  particles, the light yield is almost linear with particle energies.

#### IV. SUMMARY

In summary, a search for  $\alpha$ -decay chain  $^{108}\text{Xe} \rightarrow ^{104}\text{Te} \rightarrow ^{100}\text{Sn}$  was performed at the JAEA tandem accelerator facility using new detector technology. Based on the nonobservation of a clear pileup event, we have estimated the production cross section limit for this  $^{108}\text{Xe}$  to be less than 130 pb. Two events were observed, with decay properties

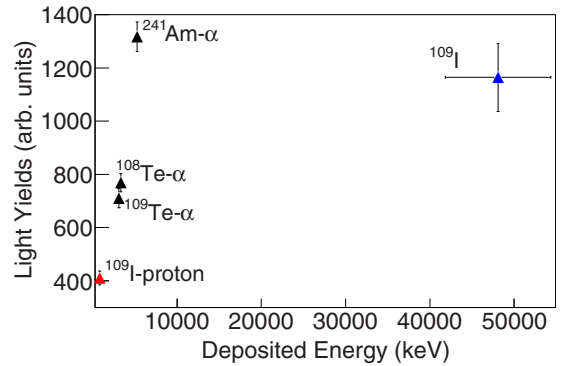


FIG. 13. A comparison of light yields of YAP:Ce crystal for different types of particles with different energies is shown.

consistent with those reported by the ANL group [10]. Our result would lead to  $T_{1/2} < 4$  ns for  $^{104}\text{Te}$  and therefore to a very large  $W_\alpha > 59$ . It is, however, possible that both events are due to  $\beta$  decays from more abundant radioactivities, and we cannot unambiguously attribute these decays to the  $^{108}\text{Xe}$  decay chain. Clearly a new experiment is needed to conclusively measure the decay properties of  $^{104}\text{Te}$ . The detection techniques proposed here can be used with electromagnetic separators using both fusion-evaporation or fragmentation reactions. A new type of scintillation detector utilizing a YAP:Ce crystal and a position sensitive PMT was developed and tested. It was applied for the first time as an implantation-decay detector. The detector was able to measure recoil-decay correlations between implanted radioactive ions and their subsequent decay, making it a viable alternative to double-sided silicon strip detectors, for experiments where fast response is more important than energy resolution. We have demonstrated that short-lived radioactivity such as, e.g., proton emission of  $^{109}\text{I}$ , can be measured, and standard correlation techniques between consecutive members of the decay chain can be implemented. A good demonstration of the capabilities of this detector was the detection of one event of the  $\alpha$ -decay chain  $^{109}\text{Xe} \rightarrow ^{105}\text{Te} \rightarrow ^{101}\text{Sn}$ , which was also correlated to its preceding ion implantation in the same pixel.

The light yield responses to different species of charged particles, e.g., protons,  $\alpha$  particles, and heavy ions, were measured, which will enable improvement of the design of these detectors for future implementations. The thin position-sensitive YAP:Ce detector shows excellent performance as an implant detector and the ability to make correlations between ion implantations and decays. It can be used in experiments where conventional DSSD detectors are too slow or may suffer from radiation damage due to high implantation rates. We also pursued the implementation of a thick detector for  $\beta$  decay studies [25,26].

#### ACKNOWLEDGMENTS

This work was supported in part by the Office of Nuclear Physics, U.S. Department of Energy under Grants No. DE-FG02-96ER40983 (UTK) and No. DE-AC05-00OR22725 (ORNL), by the National Nuclear Security Administration under the Stewardship Science Academic Alliances pro-

gram through DOE Grant No. DE-NA0002132, in part by the REIMEI research program of ASRC, JAEA, JSPS KAKENHI, Grant No. 26887048, and by the Science and

Technology Facilities Council (STFC) of the United Kingdom and the National Science Center of Poland, under Contract No. UMO-2015/17/B/ST2/00581.

- 
- [1] R. D. Macfarlane and A. Siivola, *Phys. Rev. Lett.* **14**, 114 (1965).
- [2] D. Schardt, T. Batsch, R. Kirchner, O. Klepper, W. Kurcewicz, E. Roeckl, and P. Tidemand-Petersson, *Nucl. Phys. A* **368**, 153 (1981).
- [3] Z. Janas, C. Mazzocchi, L. Batist, A. Blazhev, M. Górska, M. Kavatsyuk, O. Kavatsyuk, R. Kirchner, A. Korgul, M. La Commara *et al.*, *Eur. Phys. J. A* **23**, 197 (2005).
- [4] D. Seweryniak, K. Starosta, C. N. Davids, S. Gros, A. A. Hecht, N. Hoteling, T. L. Khoo, K. Lagergren, G. Lotay, D. Peterson, A. Robinson, C. Vaman, W. B. Walters, P. J. Woods, and S. Zhu, *Phys. Rev. C* **73**, 061301(R) (2006).
- [5] I. G. Darby, R. K. Grzywacz, J. C. Batchelder, C. R. Bingham, L. Cartegni, C. J. Gross, M. Hjorth-Jensen, D. T. Joss, S. N. Liddick, W. Nazarewicz *et al.*, *Phys. Rev. Lett.* **105**, 162502 (2010).
- [6] S. N. Liddick, R. Grzywacz, C. Mazzocchi, R. D. Page, K. P. Rykaczewski, J. C. Batchelder, C. R. Bingham, I. G. Darby, G. Drafta, C. Goodin, C. J. Gross, J. H. Hamilton, A. A. Hecht, J. K. Hwang, S. Ilyushkin, D. T. Joss, A. Korgul, W. Królas, K. Lagergren, K. Li, M. N. Tantawy, J. Thomson, and J. A. Winger, *Phys. Rev. Lett.* **97**, 082501 (2006).
- [7] C. Xu and Z. Ren, *Phys. Rev. C* **74**, 037302 (2006).
- [8] M. Karny, R. K. Grzywacz, J. C. Batchelder, C. R. Bingham, C. J. Gross, K. Hagino, J. H. Hamilton, Z. Janas, W. D. Kulp, J. W. McConnell, M. Momayezi, A. Piechaczek, K. P. Rykaczewski, P. A. Semmes, M. N. Tantawy, J. A. Winger, C. H. Yu, and E. F. Zganjar, *Phys. Rev. Lett.* **90**, 012502 (2003).
- [9] R. Grzywacz, *Nucl. Instrum. Methods Phys. Res., Sect. B* **204**, 649 (2003).
- [10] K. Auranen, D. Seweryniak, M. Albers, A. D. Ayangeakaa, S. Bottoni, M. P. Carpenter, C. J. Chiara, P. Copp, H. M. David, D. T. Doherty, J. Harker, C. R. Hoffman, R. V. F. Janssens, T. L. Khoo, S. A. Kuvin, T. Lauritsen, G. Lotay, A. M. Rogers, J. Sethi, C. Scholey, R. Talwar, W. B. Walters, P. J. Woods, and S. Zhu, *Phys. Rev. Lett.* **121**, 182501 (2018).
- [11] W. Reisdorf, *Z. Phys. A* **300**, 227 (1981).
- [12] A. Korgul, K. P. Rykaczewski, C. J. Gross, R. Grzywacz, S. N. Liddick, C. Mazzocchi, J. C. Batchelder, C. R. Bingham, I. G. Darby, C. Goodin, J. H. Hamilton, J. K. Hwang, S. V. Ilyushkin, W. Królas, and J. A. Winger, *Phys. Rev. C* **77**, 034301 (2008).
- [13] M. Alshudifat, R. Grzywacz, and S. Paulauskas, *Physics Procedia* **66**, 445 (2015).
- [14] B. Crider, C. Prokop, S. Liddick, M. Al-Shudifat, A. Ayangeakaa, M. Carpenter, J. Carroll, J. Chen, C. Chiara, H. David *et al.*, *Phys. Lett. B* **763**, 108 (2016).
- [15] M. A. Blackston, F. Habte, and P. A. Hausladen, in *Nuclear Science Symposium Conference Record, 2008, NSS'08, IEEE* (IEEE, Piscataway, NJ, 2008), pp. 4995–4998.
- [16] X. Zhang, J. P. Hayward, J. W. Cates, P. A. Hausladen, M. A. Laubach, J. E. Sparger, and S. B. Donnal, *Appl. Radiat. Isot.* **70**, 1485 (2012).
- [17] J. W. Cates, J. Hayward, X. Zhang, P. Hausladen, and B. Dabbs, *IEEE Trans. Nucl. Sci.* **59**, 1750 (2012).
- [18] M. Moszyński, M. Kapusta, D. Wolski, W. Klamra, and B. Cederwall, *Nucl. Instrum. Methods Phys. Res., Sect. A* **404**, 157 (1998).
- [19] XIA, Digital Gamma Finder (DGF) PIXIE-16 manuals, 2009 (unpublished).
- [20] H. Ikezoe, T. Ikuta, S. Mitsuoka, S. Hamada, Y. Nagame, I. Nishinaka, Y. Tsukada, Y. Oura, and T. Ohtsuki, *Nucl. Instrum. Methods Phys. Res., Sect. B* **126**, 340 (1997).
- [21] C. Mazzocchi, R. Grzywacz, S. N. Liddick, K. P. Rykaczewski, H. Schatz, J. C. Batchelder, C. R. Bingham, C. J. Gross, J. H. Hamilton, J. K. Hwang, S. Ilyushkin, A. Korgul, W. Królas, K. Li, R. D. Page, D. Simpson, and J. A. Winger, *Phys. Rev. Lett.* **98**, 212501 (2007).
- [22] T. Faestermann, A. Gillitzer, K. Hartel, P. Kienle, and E. Nolte, *Phys. Lett. B* **137**, 23 (1984).
- [23] E. Slunga, B. Cederwall, E. Ideguchi, A. Kerek, W. Klamra, J. Van der Marel, D. Novak, and L.-O. Norlin, *Nucl. Instrum. Methods Phys. Res., Sect. A* **469**, 70 (2001).
- [24] K.-H. Schmidt, C.-C. Sahn, K. Pielenz, and H.-G. Clerc, *Z. Phys. A* **316**, 19 (1984).
- [25] R. Grzywacz, RIKEN Accelerator Report **51**, 150 (2018).
- [26] R. Yokoyama, M. Singh, R. Grzywacz, A. Keeler, T. T. King, J. Agramunt, N. T. Brewer, S. Go, J. Heideman, J. Liu, S. Nishimura, P. Parkhurst, V. H. Phong, M. M. Rajabali, B. C. Rasco, K. P. Rykaczewski, D. W. Stracener, J. L. Tain, A. Tolosa-Delgado, K. Vaigneur, and M. Wolińska-Cichočka, *Nucl. Instrum. Methods Phys. Res., Sect. A* **937**, 93 (2019).